Synchronicity transitions determine connection fluctuations in a model of coupled oscillators with plasticity

Satoshi Kuroki a,*, Kenji Mizuseki a

a Department of Physiology, Osaka Metropolitan University Graduate School of Medicine
Asahimachi 1-4-3, Abeno-ku, Osaka, 545-8585, Japan
+81-6-6645-3717

* Corresponding author.
E-mail address: skuroki@omu.ac.jp

Abstract

Sleep and rest are crucial for knowledge reorganization and creativity. During these periods, synapses between neurons are plastically altered and neuronal activities are collectively synchronized, accompanied by large differences in excitation-inhibition (EI) balance. These processes are assumed to be dissimilar from the learning process during task engagement. The detailed mechanism of how synchronized neuronal activities modify neural circuits via plasticity has yet to be fully understood. The Kuramoto model is utilized to study the collective synchronization of oscillators, including neurons. We previously proposed the EI-Kuramoto model, in which the EI balance was implemented in the Kuramoto model. The model alters its synchronicity based on the EI balance of the interaction strength. In this study, we developed this EI-Kuramoto model by implementing plasticity, leading to the plastic EI-Kuramoto (pEI-Kuramoto) model. Models with high inhibition displayed desynchronized dynamics and consistent connection strengths. Models with low inhibition exhibited bistable dynamics between synchronized and desynchronized states and fluctuation of interaction strengths in middle strength connections, while the strongest connections remained stable. These results, stabilizing a few strong connections and fluctuating the other connections in low inhibition conditions, could facilitate knowledge abstraction and reorganization. Our findings shed light on how varying inhibitory effects influence network stability and coupling, offering deeper insights into synaptic networks and knowledge reshaping.

Introduction

Empirical evidence suggests that the activity of the brain during sleep and rest promotes the reorganization of the neural circuit, leading to abstracting knowledge and creating new ideas (Landmann et al., 2014; Lewis et al., 2018). This reorganization is considered to be a different

process from learning processes in active awake. Synaptic plasticity during sleep and rest modifies neural structure and functionality and improves task performance (Goto et al., 2021; Norimoto et al., 2018). On the other hand, collective neuronal oscillations synchronize during sleep and rest while they desynchronize during task engagement (Harris and Thiele 2011). In the synchronized and desynchronized states, the inhibitory neuronal activity and synaptic conductance significantly diverge from those of excitatory neurons (Alfonsa et al., 2022; Haider et al., 2013; Miyawaki & Diba, 2016; Mizuseki & Buzsáki, 2013), consequently causing shifts in the Excitatory-Inhibitory (EI) balance. These observations indicate how much collective neuronal synchronization controlled by the EI balance and synaptic plasticity during sleep and rest can affect cognitive functions. However, the detailed mechanisms by which the synchronized state reorganizes neural network structure remain unclear.

Collective synchronization of oscillators, including neurons, has been explored through modeling coupled oscillators. The Kuramoto model stands as the simplest model among them (Kuramoto, 1984, 1975). Numerous variants of the Kuramoto model have been examined (Acebrón et al., 2005). Some variants incorporate features such as plasticity, which allows for changes in the interaction strength between oscillators (Aoki & Aoyagi, 2009; Bronski et al., 2017; Fialkowski et al., 2023; Ha et al., 2018, 2016; Niyogi & English, 2009; Park et al., 2021; Picallo & Riecke, 2011; Poyato, 2019; Ren & Zhao, 2007; Seliger et al., 2002). Furthermore, in the Kuramoto model, the EI balance is conceptualized as a balance between two conflicting forces (EI-Kuramoto model), leading to synchronized oscillations induced through feedback mechanisms (Montbrió & Pazó, 2018) and transfer between different dynamic states, synchronized, bistable, and desynchronized, by modulating the EI-balance (Kuroki & Mizuseki, 2024).

In the current research, we refined the EI-Kuramoto model by integrating Hebbian and homeostatic plasticity into the interaction strengths among oscillator units (referring to plastic EI, pEI-Kuramoto model). We observed that the network maintains robustness and minimal fluctuations when the inhibition is strong, corresponding to the desynchronized state. Conversely, with weaker inhibition, corresponding to the bistable state, connections of moderate interaction strengths tend to fluctuate, although connections with strong strengths remain stable. These findings concerning the network dynamics of the pEI-Kuramoto model may offer significant insights into the mechanisms of synaptic networks and the knowledge process reconstruction during sleep and rest.

Methods

pEI-Kuramoto model

The original Kuramoto model (Acebrón et al., 2005; Kuramoto, 1984, 1975) is expressed as

$$\frac{d\theta_j(t)}{dt} = \omega_j + \frac{K}{N}\sum_{k}^{N}\sin(\theta_k(t) - \theta_j(t)) \quad (1),$$

where $\theta_j(t)$ is the phase of unit j at time t, ω_j is the natural frequency of unit j following a probability distribution $g(\omega)$, N is the number of units, and K is the interaction strength among the oscillation units. In the original Kuramoto model, K is constantly and uniformly applied to all pairs of unit interactions. The order parameter R and the mean phase ψ are then calculated from the mean vector of the oscillators

$$Re^{i\psi} = \frac{1}{N}\sum_{j}^{N} e^{i\theta_j} \quad (2),$$

where i is an imaginary unit.

Given Eq (2), Eq (1) becomes

$$\frac{d\theta_j}{dt} = \omega_j + KR\sin(\psi - \theta_j) \quad (3).$$

In our previous EI-Kuramoto model (Kuroki & Mizuseki, 2024), the oscillation units are categorized into two groups: excitatory and inhibitory units, referred to as excUnits and inhUnits, respectively. Employing these specific terms clarified that the units represent excitatory and inhibitory factors in the model, distinguishing them from actual neurons or synapses. The interaction strength of sine-wave functions with zero phase lag is characterized by purely attractive interactions in excUnits and purely repulsive interactions in inhUnits. Hence, the terms "excitatory" and "inhibitory" are used interchangeably with "attractive" and "repulsive," respectively. The interaction strength K is divided into four types, K_{ee} (attractive strength between excUnits), K_{ii} (repulsive strength between inhUnits), K_{ei} (attractive strength from excUnits to inhUnits), and K_{ie} (repulsive strength from inhUnits to excUnits). Eq (3) becomes

$$\frac{d\theta_{j,exc}}{dt} = \omega_{j,exc} + K_{ee}R_{exc}\sin(\psi_{exc} - \theta_{j,exc}) - K_{ie}R_{inh}\sin(\psi_{inh} - \theta_{j,exc}) \quad (4)$$

for excUnits, and

$$\frac{d\theta_{j,inh}}{dt} = \omega_{j,inh} + K_{ei}R_{exc}\sin(\psi_{exc} - \theta_{j,inh}) - K_{ii}R_{inh}\sin(\psi_{inh} - \theta_{j,inh}) \quad (5)$$

for inhibUnits. exc and inh represent parameters for excUnits and inhUnits, respectively. The order parameter and mean phase of each excUnits and inhUnits are

$$R_{exc}e^{i\psi_{exc}} = \frac{1}{N_{exc}}\sum_{j}^{N_{exc}} e^{i\theta_{j,exc}} \quad (6)$$

and

$$R_{inh}e^{i\psi_{inh}} = \frac{1}{N_{inh}}\sum_{j}^{N_{inh}} e^{i\theta_{j,inh}} \quad (7).$$

In this study, the pEI-Kuramoto model, the K_{ee} values are distributed and plastic. The initial distribution of K_{ee} follows the Gaussian distribution $g(K_{ee}) \sim \mathcal{N}(\mu_{Kee}/N_{exc}, (\sigma_{Kee}/N_{exc})^2)$, where μ_{Kee} is mean and σ_{Kee} is standard deviation of the K_{ee} distribution. These are scaled with

an inverse of N_{exc}. The other K values, K_{ii}, K_{ei}, and K_{ie}, are distinct positive real numbers uniformly and constantly applicable across all units. Eq (4) becomes

$$\frac{d\theta_{j,exc}}{dt} = w_{j,exc} + \sum_{k}^{N_{exc}} K_{ee,kj} \sin(\theta_{k,exc} - \theta_{j,exc}) - K_{ie} R_{inh} \sin(\psi_{inh} - \theta_{j,exc}) \quad (8).$$

For all simulations in this study, $N_{exc} = 80$, $N_{inh} = 20$, total simulation duration $T = 50$ s, time step $dt = 0.01$ s, $g(\omega)$ of both excUnits and inhUnits followed Gaussian distribution $g(\omega) \sim \mathcal{N}(0, 0.01)$. The range of time to evaluate the mean of order parameters, R_{exc} and R_{inh}, is from $T/2$ to T to exclude initial fluctuations. In Figure 2–5, K_{ii} and K_{ie} were integrated as the same parameter to simplify the simulation

$$K_i = K_{ie} = K_{ii} \quad (9).$$

K_{ee} values were modulated depending on the Hebbian potentiation and homeostatic regularization rules.

Hebbian potentiation plasticity was implemented as an exponential function:

$$\frac{dK_{ee,kj}}{dt} = \alpha exp(-\gamma \Delta\theta_{kj}) \quad (10).$$

$K_{ee,kj}$ is connection strength between ExcUnits k and j, α is a learning rate for the Hebbian plasticity. Note that α should scale proportionally with an inverse of N_{exc} as $\alpha \propto 1/N_{exc}$ to maintain consistency across different distribution sizes. γ determines a sharpness exponential decay from the peak. $\Delta\theta_{kj}(t)$ is a phase difference between ExcUnit k and j at time t

$$\Delta\theta_{kj} = (\theta_{k,exc} - \theta_{j,exc})(-\pi \leq \Delta\theta_{kj} < \pi) \quad (11).$$

Implementation of Hebbian plasticity with cosine function was

$$\frac{dK_{ee,kj}}{dt} = \frac{\alpha}{2}\{\cos(\Delta\theta_{kj}) + 1\} \quad (12).$$

After the Hebbian plastic changes, the K_{ee} were rescaled with the homeostatic regularization plasticity rule to prevent overpotentiation. The plasticity was implemented as

$$\hat{K}_{ee,kj} = \frac{\hat{\sigma}_{K_{ee}}}{S[K_{ee}]}(K_{ee,kj} - E[K_{ee}]) + \hat{\mu}_{K_{ee}}$$

$$K_{ee,kj} \leftarrow \beta \hat{K}_{ee,kj} + (1 - \beta) K_{ee,kj} \quad (13).$$

$\hat{K}_{ee,kj}$ is scaled $K_{ee,kj}$ adjusting to initial μ_{Kee} and σ_{Kee} settings, $\hat{\mu}_{Kee} = \mu_{Kee}/N_{exc}$, $\hat{\sigma}_{Kee} = \sigma_{Kee}/N_{exc}$. $E[K_{ee}](t)$ and $S[K_{ee}](t)$ is calculated mean and standard deviation of the K_{ee} distribution at t before the regularization. β is a learning rate for the regularization plasticity. This process rescales the K_{ee} distribution towards distribution with mean $\hat{\mu}_{Kee}$ and standard deviation $\hat{\sigma}_{Kee}$.

Cyclic inhibitory modulation

In Figure 5, K_i is modulated as a sine function

$$K_i = A_s \sin(\omega_s t) + C_s \quad (14),$$

where A_s (= 0.32), ω_s (= 0.004π), and C_s (= 1.4) are the amplitude, frequency, and baseline constant for the sine modulation, respectively.

Statistics

$E[\cdot]_t$ (also $E\{\cdot\}_t$) and $S[\cdot]_t$ is the mean and the standard deviation over time. $E[\cdot]_n$ and $S[\cdot]_n$ is the mean and the standard deviation among unit pairs. $\cdot$ represents a certain variable. For Figure 5B lower panel, the time window ($\pm$15 sec from the time point) was set.

Dip test (Hartigan & Hartigan, 1985) is calculated by Python diptest library (https://github.com/RUrlus/diptest). Briefly, the dip value is the maximum distance between the actual data distribution and that of fitting result to the monomodal Gaussian distribution. If the data distribution is close to the monomodal Gaussian distribution, the dip value is low. If bimodal, the value is high.

Results

First, we investigated the impact of the distributed K_{ee} interaction strengths on the dynamics of the pEI-Kuramoto model, referred to as dynamic states. The association between the dynamic states and constant values of each K has been scrutinized in our previous study (Kuroki & Mizuseki, 2024). In this study, K_{ee} was distributed following a Gaussian distribution with mean μ_{Kee} and standard deviation σ_{Kee}. σ_{Kee} was set to 0, 1/100, and 1/20 of μ_{Kee} (Fig 1A). The collective synchronization was assessed by the order parameter R, representing the magnitude of the average vector among oscillator units. Roughly, irrespective of the standard deviation, all systems with a distributed K_{ee} also displayed synchronized (high R), bistable (alternating high and low R), and desynchronized (low R) dynamics like those observed with constant K values (Fig 1B).

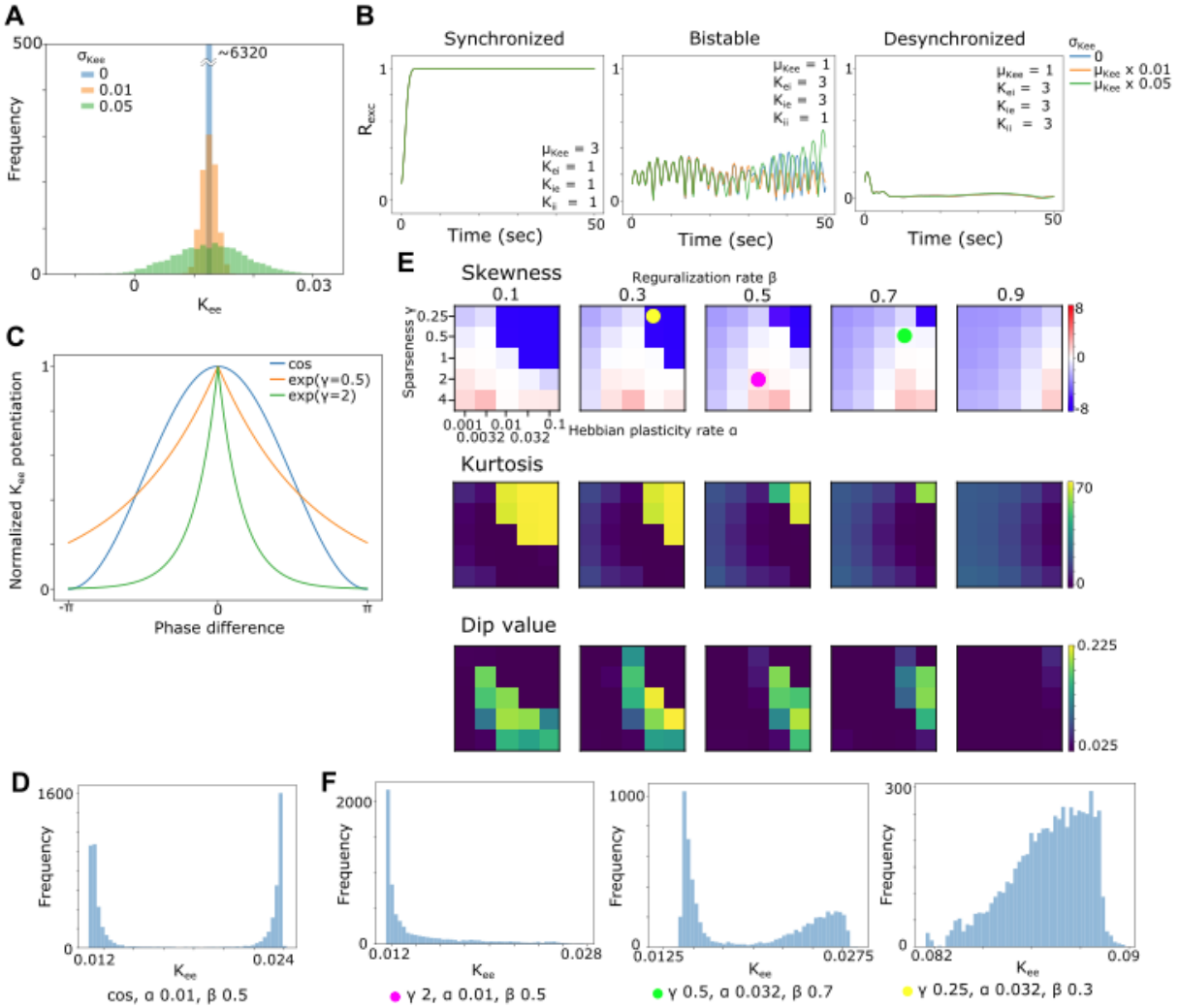

Figure 1 EI-Kuramoto model with distributed K_{ee} and plasticity
(A) Distribution of K_{ee} values with different σ_{Kee}. μ_{Kee} = 1, N_{exc} = 80. (B) R_{exc} time traces of synchronized, bistable, and desynchronized state with each σ_{Kee}. (C) Hebbian potentiation plasticity rules. K_{ee} value of each unit pair is potentiated based on the phase distance between the units. (D) K_{ee} distribution with the cosine Hebbian plasticity rule. (E) Validation of K_{ee} distribution with various plasticity parameters. Skewness (upper panels), kurtosis (middle), and dip values (lower). K values for the evaluation were μ_{Kee} = 1, σ_{Kee} = 0.01, K_{ei} = 3, K_{ie} = 3, K_{ii} = 3, corresponding to a desynchronized state. (F) K_{ee} distribution of exponential Hebbian plasticity rules with various parameter settings. The magenta, green, and yellow circles correspond to the parameter setting on (E).

Next, we incorporated plasticity into K_{ee}, following the Hebbian plasticity rule (see Materials and Methods). Among the various methods available to implement Hebbian plasticity in the Kuramoto model, we initially opted for the simplest method, the cosine (or sine) function (Fig 1C cos, see Materials and Methods) (Aoki & Aoyagi, 2009; Bronski et al., 2017; Fialkowski et al., 2023; Niyogi & English, 2009; Ren & Zhao, 2007; Seliger et al., 2002). The K_{ee} distribution was rescaled to reflect the initial mean and standard deviation to prevent overpotentiation

(homeostatic regularization plasticity, see Materials and Methods). Under the cosine rule and desynchronized state (μ_{Kee} = 1, σ_{Kee} = 0.01, K_{ei} = 3, K_{ie} = 3, K_{ii} = 3), unit pairs of closer phases acquire a greater K_{ee}. Under this rule, the distribution of K_{ee} resulted in a bimodal configuration (Fig 1D).

Furthermore, we utilized an exponential function as the Hebbian plasticity rule to adjust the decay rate (γ) of the gain for the phase difference (Fig 1C, exp). We subjected this plasticity rule to a range of parameter sets, examining the distribution of K_{ee} in a desynchronized state. These distributions initially followed a Gaussian pattern but transitioned to bimodal or skewed formations (Fig 1E and F). Notably, the biological brain displays a long-tailed skewed distribution in synaptic weights (Buzsáki & Mizuseki, 2014; Mizuseki & Buzsáki, 2013). With this view, we opted for a parameter set that yielded a long-tailed skewed distribution (Fig 1F, magenta circle). Plastic changes in K_{ee} were observed over time in synchronized, bistable, and desynchronized states (Supplementary video 1–3).

Inhibition exhibits significant variability across different brain states, resulting in modifications to the EI balance (Harris & Thiele, 2011; Nobre & Kastner, 2014). Herein, we altered the EI balance of the pEI-Kuramoto model by manipulating the interaction strength from inhUnits. We integrated K_{ie} and K_{ii} into K_i to simplify the simulation, following the approach used in our previous study (Kuroki & Mizuseki, 2024). We then examined the relationship between K_i values and K_{ee} fluctuations. The fluctuations were quantified as the standard deviation of K_{ee} over time ($S[K_{ee}]_t$). We observed that as K_i increases, the average $S[K_{ee}]_t$ across unit pairs ($E\{S[K_{ee}]_t\}_n$) also increases, reaching a peak at K_i = 0.7. Beyond this point, it decreases and eventually stabilizes around K_{ii} = 1.5 (see Fig 2A). The standard deviation of $S[K_{ee}]_t$ among unit pairs ($S\{S[K_{ee}]_t\}_n$) exhibited a consistent increase (Fig 2B). By analyzing the time course of R_{exc} (Fig 2C and D), we can determine the dynamic state of the system as described in our previous study (Kuroki & Mizuseki, 2024). For K_i values below 0.5, the system was in a synchronized state characterized by high $E[R_{exc}]_t$ and low $S[R_{exc}]_t$. In contrast, for K_i values above 1.5, the system enters a desynchronized state, characterized by low $E[R_{exc}]_t$ and $S[R_{exc}]_t$. Within the range of $0.5 < K_i < 1.5$, the system displays a bistable state with high $S[R_{exc}]_t$. Notably, $S[K_{ee}]_t$ was significantly high during this bistable state (Fig 2A and D).

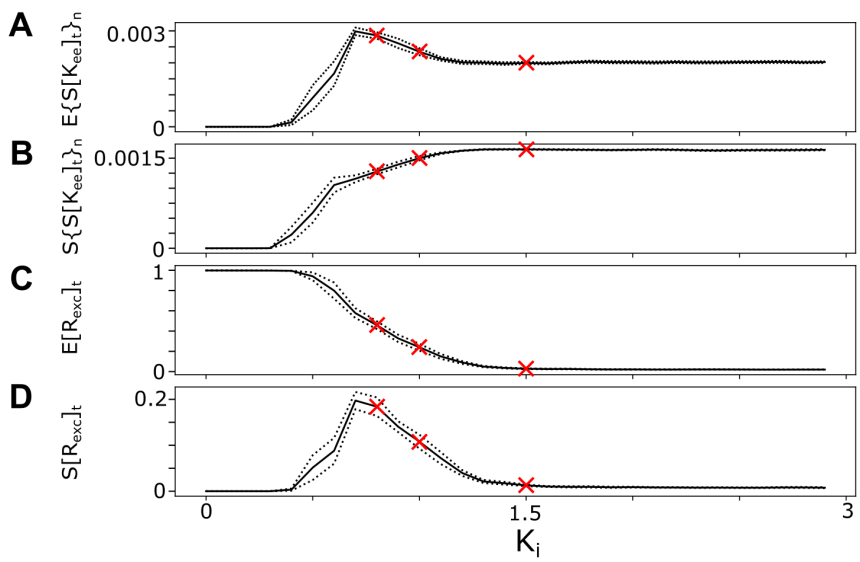

Figure 2 K_{ee} fluctuation changes with K_i modification
(A) $E\{S[K_{ee}]_t\}_n$, (B) $S\{S[K_{ee}]_t\}_n$, (C) $E[R_{exc}]_t$, and (D) $S[R_{exc}]_t$ as a function of K_i. Red crosses indicate K_i values for analyses in Figures 3 and 4.

We analyzed the behavior of individual K_{ee} connections at selected points of K_i (K_i = 0.8, 1.0, and 1.5, red crosses in Figure 2). With the decrease in K_i from 1.5 to 0.8, the fluctuation of K_{ee} appeared to increase (Figures 3A and B). Correspondingly, the histograms of $E[K_{ee}]_t$ (mean of K_{ee} over time for each unit pair) and $S[K_{ee}]_t$ also tended to shift towards higher values with the decreasing K_i (Figures 3C and D). The scatter plot of $E[K_{ee}]_t$ and $S[K_{ee}]_t$ formed a distinctive 'bow-shaped' distribution (Figure 3E). In this distribution, data points near the minimum and maximum $E[K_{ee}]_t$ values were linked to lower $S[K_{ee}]_t$ values, whereas the $S[K_{ee}]_t$ values were higher for intermediate $E[K_{ee}]_t$ values. This pattern was consistent across all distributions for different K_i values. Similar phenomena, stabilization of strong connections, were observed in the synapses of the brain (Grutzendler et al., 2002; Holtmaat et al., 2005; Matsuzaki et al., 2004).

Furthermore, it showed a trend of increasing $S[K_{ee}]_t$ levels at intermediate $E[K_{ee}]_t$ as K_i decreased (Fig 3E), indicating that K_i can regulate the fluctuations of each K_{ee} plastic connection. At high K_i in desynchronized states, connections stabilize, whereas at lower K_i in bistable states, connections of intermediate K_{ee} strength become unstable. The high K_{ee} connection remains stable with small fluctuations even when K_i is low. These dynamics appear to be a mechanism that preserves the connections of particularly strong pairs and resets pairs of moderate connection strength, facilitating the reorganization of the network structure.

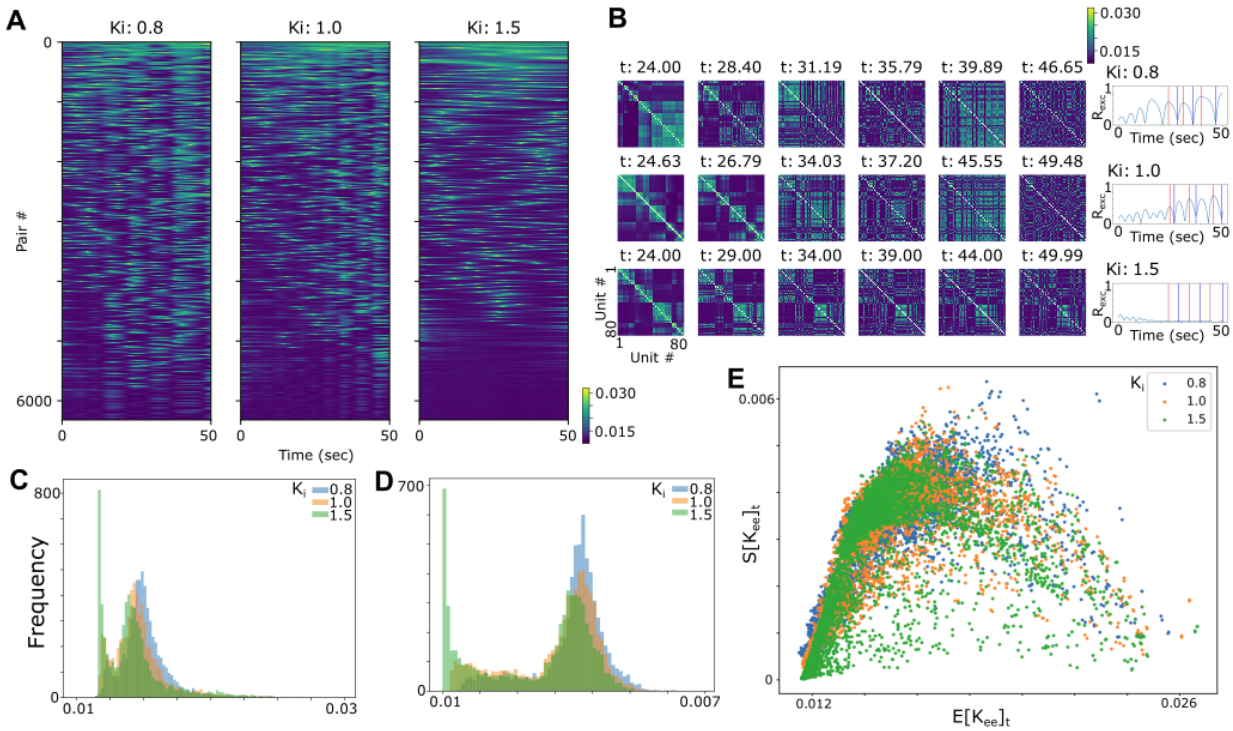

Figure 3 K_{ee} changes of pEI-Kuramoto model
(A) Time trace of each K_{ee} value sorted by $E[K_{ee}]_t$ for each K_i value. (B) The left panels show the K_{ee} value matrix at several time points (local minimum or maximum for K_i = 0.8 and 1.0, constant 0.5 s interval for K_i = 1.5). The right panels display R_{exc} traces and time points of the left K_{ee} matrices. Red and blue vertical lines are the time points (Red and blue are local maximum and local minimal, respectively, for K_i = 0.8 and 1.0). (C) $E[K_{ee}]_t$ histogram. (D) $S[K_{ee}]_t$ histogram. (E) $E[K_{ee}]_t$ vs $S[K_{ee}]_t$ scatter plot for different K_i values.

What parameters determine the positions in the distribution shown in Fig 3E? To explore the parameters involved in K_{ee} fluctuations, we colored each point in the scatter plot of Fig 3E based on the values of candidate parameters (Fig 4). The connections were roughly categorized based on whether $E[K_{ee}]_t$ exceeded 0.018 (high $E[K_{ee}]_t$ group) or not (low $E[K_{ee}]_t$ group) for statistical comparisons because the trend reverses around this point.

Regarding the differences in natural frequency (ω_{exc}) of EexUnit pairs, smaller natural frequency differences were associated with smaller $S[K_{ee}]_t$. Pairs with larger natural frequency differences tended to be in the low $E[K_{ee}]_t$ group, and the $S[K_{ee}]_t$ appears to increase with increasing natural frequency differences. On the other hand, the majority of pairs in the high $E[K_{ee}]_t$ group exhibited relatively small natural frequency differences (Fig 4A and D). The initial phase differences between pairs were also influential. In the low $E[K_{ee}]_t$ group, the initial phase differences were uniformly observed, whereas in the high $E[K_{ee}]_t$ group, many pairs exhibited small initial phase differences (Fig 4B and E). Additionally, we examined the initial connection strength of K_{ee}, which appeared to be normally distributed without noticeable bias (Fig 4C and F). As a result, pairs with small differences in natural frequency and initial phase positions maintained more

stable and larger K_{ee} values (Fig 4G and H). In contrast, the initial K_{ee} values were not a significant factor.

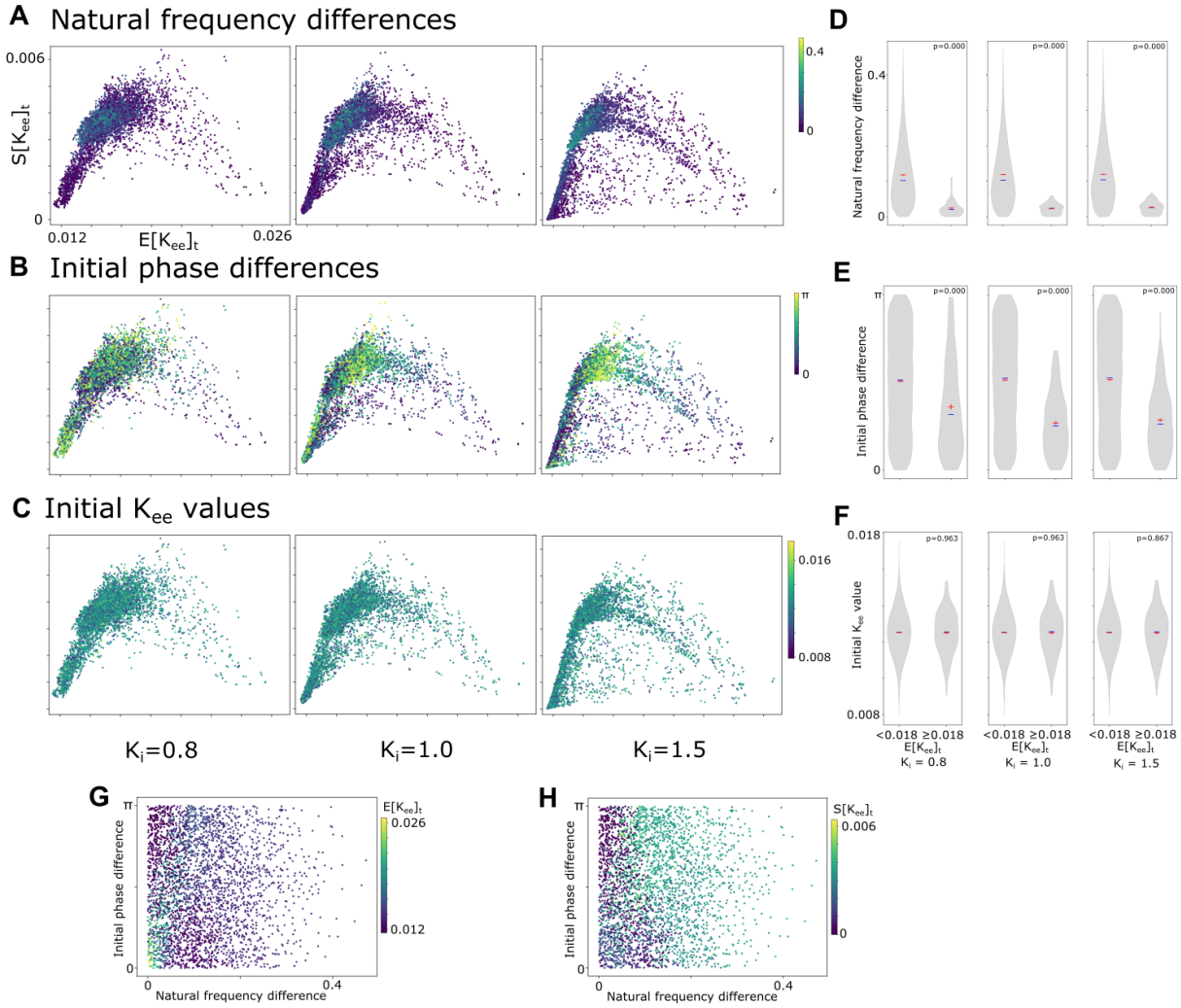

Figure 4 Factors for K_{ee} fluctuation

(A–C) $E[K_{ee}]_t$ vs $S[K_{ee}]_t$ scatter plot with color coding of (A) the natural frequency ω_{exc} differences, (B) the initial phase differences, and (C) the initial K_{ee} values across different K_i. (D–F) Violin plots provide distribution densities based on whether the threshold $E[K_{ee}]_t \geq 0.18$ or not for (D) natural frequency ω_{exc} differences, (E) initial phase differences, and (F) initial K_{ee} values across different K_i. Red and blue horizontal lines indicate mean and median, respectively. Red vertical lines indicate standard error. The numbers at top right in each panel are p-values from the Mann-Whitney U test. (G and H) Scatter plots between natural frequency differences and initial phase differences with color coding of (G) $E[K_{ee}]_t$ and (H) $S[K_{ee}]_t$ (K_i = 1.5). Mann-Whitney U test was used for statistical analysis in D-F. The numbers of unit pairs were as follows: for K_i=0.8, <0.18: n=5968, ≥0.18: n=352; for K_i=1.0, <0.18: n=5920, ≥0.18: n=400; for K_i=1.5, <0.18: n=5852, ≥0.18: n=468. The statistic results were as follows: (D, Natural frequency

difference), K_i=0.8, z=24.7, p<0.001; K_i=1.0, z=26.8, p<0.001; K_i=1.5, z=27.8, p<0.001. (E, Initial phase difference) K_i=0.8, z=9.20, p<0.001; K_i=1.0, z=16.4, p<0.001; K_i=1.5, z=16.7, p<0.001. (F, Initial K_{ee} value) K_i=0.8, z=-0.046, p=0.96; K_i=1.0, z=0.046, p=0.96; K_i=1.5, z=0.17, p=0.87.

We fluctuated K_i to emulate the sleep-wake cycle (Harris & Thiele, 2011). K_{ee} exhibited fluctuations (Fig 5A, Supplementary video 4) according to the modulation of K_i (Fig 5B Upper). R_{exc} alternated between the desynchronized and bistable states (Fig 5B middle), and $E\{S[K_{ee}]_t\}_n$ changed correspondingly (Fig 5B low). When K_i was high, the system exhibited a desynchronized state, and the $E\{S[K_{ee}]_t\}_n$ was small. Conversely, when K_i was low, the system exhibited a bistable state, and $E\{S[K_{ee}]_t\}_n$ increased. These dynamics can be seen as modeling how the circuit structure is stabilized during wakefulness and destabilized during sleep and rest, thereby promoting circuit reorganization.

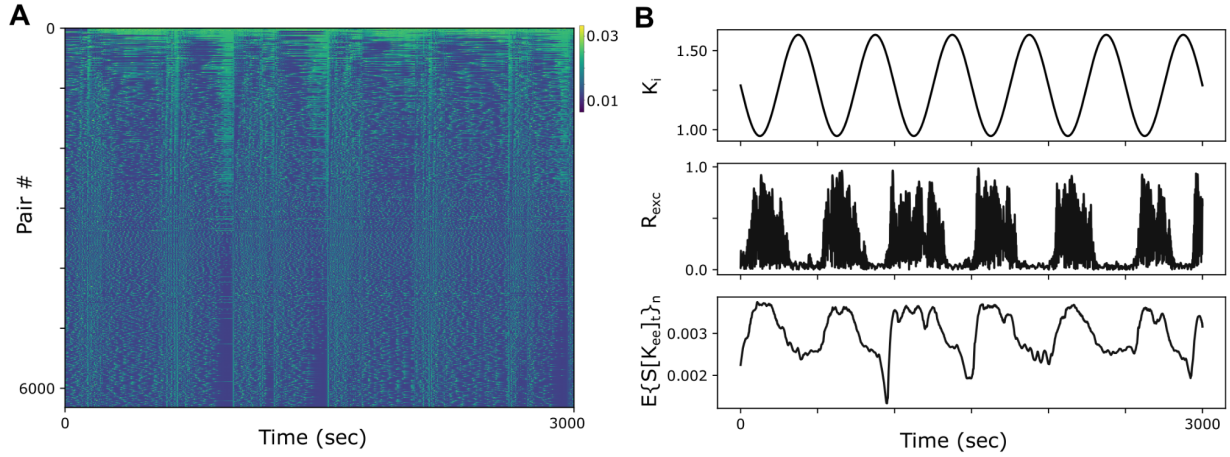

Figure 5 K_{ee} changes with K_i cyclic modulation
(A) Time trace of each K_{ee} value sorted by $E[K_{ee}]_t$. (B) Time traces of (top) K_i modulation, (middle) R_{exc}, and (low) $E\{S[K_{ee}]_t\}_n$.

Discussions

In this study, we extended the previously developed EI-Kuramoto model by incorporating plasticity, thus establishing the pEI-Kuramoto model, and analyzed its behavior. We propose that this model represents a continuous transition between stabilization and reorganization of the network connections, modulated by the desynchronized-bistable state cycle through inhibition. It serves as a framework for understanding the complex interactions between the stabilization and reorganization of neural circuits in the awake-sleep cycle.

Potential mechanism for knowledge generalization and new idea generation

The selective preservation of the robust connections in a network potentially facilitates knowledge generalization. This process has been demonstrated in artificial neural networks, known as the pruning method (Bartoldson et al., 2020; Hoefler et al., 2021). Similarly, in the brain, the selective preservation of strong synaptic connections is well-documented (Grutzendler et al., 2002; Holtmaat et al., 2005; Matsuzaki et al., 2004) and is understood through molecular mechanisms, including the dynamics of NMDA receptors (Norimoto et al., 2018; Tononi & Cirelli, 2020) and actin filaments (Kasai et al., 2010). Our findings introduce a potential mechanism for sustaining strong connections, viewed through another aspect of the dynamical system of collective oscillators. Especially if synaptic down-regulation is dominant in sleep or rest (Norimoto et al., 2018; Tononi & Cirelli, 2020), fluctuation of connection strengths can lead to weakening and initializing the connections and work as a pruning-like mechanism.

Furthermore, fluctuation in the network connection may enhance the generation of new ideas. In our model, the bistable states under conditions of low inhibition, mirroring brain dynamics during sleep and rest (Alfonsa et al., 2022; Haider et al., 2013; Miyawaki & Diba, 2016; Mizuseki & Buzsáki, 2013), promote fluctuation in the connection strengths (see Figures 3–5). This process leads to associations (synchronization) among memory elements and network reorganization, transitioning from associations between closely related elements to nearly random associations as inhibition decreases. It is proposed that sleep and rest periods enhance the generation of new ideas through neuronal circuit reorganization (Landmann et al., 2014; Lewis et al., 2018). Combined with some unknown mechanisms to evaluate and stabilize the reorganizing circuits, such as dopaminergic signals during sleep (Gomperts et al., 2015), we may approach how the new creative ideas or inexperienced problem-solving methods was generated.

Dynamics of this model

The scatter plot of $E[K_{ee}]_t$ and $S[K_{ee}]_t$ exhibited a ‘bow-shaped’ distribution (Fig 3E). We hypothesize that this pattern reflects two distinct trends. Firstly, predominantly on the left side of the scatter plot, $S[K_{ee}]_t$ increased with $E[K_{ee}]_t$. This trend appeared from the nearly independent oscillating behavior of unit pairs with weak K_{ee} connections. In contrast, the second trend, mainly observed on the right side of the plot, showed $S[K_{ee}]_t$ decreasing as $E[K_{ee}]_t$ increases. This trend indicates pairs with higher connection strength, where an increase in strength correlates with decreased variance, suggesting enhanced stability. This pattern is likely due to the stabilizing influence of strong K_{ee} interactions. In this model, there is an overlap between these two properties.

In this model, pairs with small differences in natural frequencies and initial phases tend to form strong, stable connections, while initial K_{ee} values are less significant (see Figure 4). This outcome is reasonable and straightforward. Pairs with closer natural frequencies interact more easily, and those with similar initial phase positions are more susceptible to Hebbian potentiation effects. Adjusting plasticity parameters to create a long-tailed synaptic distribution,

thereby prioritizing initial phase differences over initial K_{ee} strength, is an interesting observation. This finding could enhance our understanding of similar mechanisms in the biological brain. Hippocampal neurons that exhibited synchronized firing before learning (like small initial phase differences) are more likely to group together during learning (Dragoi and Tonegawa 2011). However, it is not yet clear if these neurons also have similar firing frequencies, as seen with natural frequencies in our model. This parallel provides a new perspective, deepening our understanding of neuronal behavior.

Limitation

The Kuramoto model, while offering foundational insights, is considerably more simplistic than true neuronal behavior and has certain limitations. First, our model simplifies neuronal interactions to mere attractive and repulsive forces, overlooking the pulse-like nature and intricate coupling relationships in actual neurons (Izhikevich, 2010). Second, the model underrepresents neuroplasticity complexity such as influences of neurotransmitters and internal conditions (Brzosko et al., 2019), and disregards plasticity in inhibitory neurons (Chiu et al., 2019; Wu et al., 2022). Third, the model fails to incorporate anatomical biases in connection strengths found in actual neural circuits, suggesting a need for future models to include such biases (Andersen et al., 2006; Braitenberg & Schüz, 1998). Lastly, the model does not differentiate between neurological states like full wakefulness, non-REM sleep, and REM sleep, believed to play unique roles in learning and neural reorganization (Landmann et al. 2014; Lewis, Knoblich, and Poe 2018). Addressing these limitations is essential for a more accurate and comprehensive understanding of neural dynamics and plasticity.

Future direction

In this study, we observed behavior where strong connections were retained and other connections were randomly perturbed at low inhibition. For creating ideas, a mechanism to evaluate and stabilize randomly reorganized circuits may be required. This mechanism is not yet fully understood, but we think that the activity of dopamine during rest (Gomperts et al., 2015) could be a pivotal factor in the mechanism.

The prevailing hypothesis suggests that memory content is initially stored in the hippocampus and gradually transitions to the cerebral cortex during sleep (Klinzing et al., 2019). It raises the question of how the synchronicity changes affect the interaction between the two different networks, such as the hippocampus and the cerebral cortex.

Our model did not specifically consider the dimensionality of information, but understanding how the brain represents and selects multidimensional information is a crucial aspect of cognition (Barak, 2017). We must consider what biases, interactions, and plasticity rules are needed to represent and select various multidimensional information from the external world.

Code Availability Statement

The scripts for this study can be found in the Google Colaboratory: https://colab.research.google.com/drive/1v8JF97G9YdwUOh_Wuh9i_TvuGa42fLAu?usp=sharing

Supplementary material

Supplemental video 1
Synchronized state: K_{ee}=3, K_{ei}=1, K_{ie}=1, K_{ii}=1, γ=2, α=0.01, β=0.5; playback speed: ×1.

Supplemental video 2
Bistable state: K_{ee}=1, K_{ei}=3, K_{ie}=3, K_{ii}=1, γ=2, α=0.01, β=0.5; playback speed: ×1.

Supplemental video 3
Desynchronized state: K_{ee}=1, K_{ei}=3, K_{ie}=3, K_{ii}=3, γ=2, α=0.01, β=0.5; playback speed: ×1.

Supplemental video 4
Cyclic inhibitory modulation K_i; playback speed: ×20.

References

Acebrón, J. A., Bonilla, L. L., Pérez Vicente, C. J., Ritort, F., & Spigler, R. (2005). The Kuramoto model: A simple paradigm for synchronization phenomena. *Reviews of Modern Physics*, *77*(1), 137–185. https://doi.org/10.1103/RevModPhys.77.137

Alfonsa, H., Burman, R. J., Brodersen, P. J. N., Newey, S. E., Mahfooz, K., Yamagata, T., Panayi, M. C., Bannerman, D. M., Vyazovskiy, V. V., & Akerman, C. J. (2022). Intracellular chloride regulation mediates local sleep pressure in the cortex. *Nature Neuroscience*, *26*(1), 64–78. https://doi.org/10.1038/s41593-022-01214-2

Andersen, P., Morris, R., Amaral, D., Bliss, T., & O'Keefe, J. (Eds.). (2006). *The hippocampus book*. Oxford University Press. https://doi.org/10.1093/acprof:oso/9780195100273.001.0001

Aoki, T., & Aoyagi, T. (2009). Co-evolution of phases and connection strengths in a network of

phase oscillators. *Physical Review Letters*, *102*(3), 034101. https://doi.org/10.1103/PhysRevLett.102.034101

Barak, O. (2017). Recurrent neural networks as versatile tools of neuroscience research. *Current Opinion in Neurobiology*, *46*, 1–6. https://doi.org/10.1016/j.conb.2017.06.003

Bartoldson, B., Morcos, A., Barbu, A., & Erlebacher, G. (2020). The generalization-stability tradeoff in neural network pruning. In H. Larochelle, M. Ranzato, R. Hadsell, M. F. Balcan, & H. Lin (Eds.), *Advances in Neural Information Processing Systems* (Vol. 33, pp. 20852–20864). Curran Associates, Inc.

Braitenberg, V., & Schüz, A. (1998). *Cortex: Statistics and geometry of neuronal connectivity*. Springer Berlin Heidelberg. https://doi.org/10.1007/978-3-662-03733-1

Bronski, J. C., He, Y., Li, X., Liu, Y., Sponseller, D. R., & Wolbert, S. (2017). The stability of fixed points for a Kuramoto model with Hebbian interactions. *Chaos* , *27*(5), 053110. https://doi.org/10.1063/1.4983524

Brzosko, Z., Mierau, S. B., & Paulsen, O. (2019). Neuromodulation of spike-timing-dependent plasticity: Past, present, and future. *Neuron*, *103*(4), 563–581. https://doi.org/10.1016/j.neuron.2019.05.041

Buzsáki, G., & Mizuseki, K. (2014). The log-dynamic brain: how skewed distributions affect network operations. *Nature Reviews. Neuroscience*, *15*(4), 264–278. https://doi.org/10.1038/nrn3687

Chiu, C. Q., Barberis, A., & Higley, M. J. (2019). Preserving the balance: diverse forms of long-term GABAergic synaptic plasticity. *Nature Reviews. Neuroscience*, *20*(5), 272–281. https://doi.org/10.1038/s41583-019-0141-5

Fialkowski, J., Yanchuk, S., Sokolov, I. M., Schöll, E., Gottwald, G. A., & Berner, R. (2023). Heterogeneous nucleation in finite-size adaptive dynamical networks. *Physical Review Letters*, *130*(6), 067402. https://doi.org/10.1103/PhysRevLett.130.067402

Gomperts, S. N., Kloosterman, F., & Wilson, M. A. (2015). VTA neurons coordinate with the

hippocampal reactivation of spatial experience. *ELife*, *4*, e05360. https://doi.org/10.7554/eLife.05360

Goto, A., Bota, A., Miya, K., Wang, J., Tsukamoto, S., Jiang, X., Hirai, D., Murayama, M., Matsuda, T., McHugh, T. J., Nagai, T., & Hayashi, Y. (2021). Stepwise synaptic plasticity events drive the early phase of memory consolidation. *Science*, *374*(6569), 857–863. https://doi.org/10.1126/science.abj9195

Grutzendler, J., Kasthuri, N., & Gan, W.-B. (2002). Long-term dendritic spine stability in the adult cortex. *Nature*, *420*(6917), 812–816. https://doi.org/10.1038/nature01276

Ha, S. Y., Lee, J., Li, Z., & Park, J. (2018). Emergent dynamics of Kuramoto oscillators with adaptive couplings: Conservation law and fast learning. *SIAM Journal on Applied Dynamical Systems*, *17*(2), 1560–1588. https://doi.org/10.1137/17M1124048

Ha, S. Y., Noh, S. E., & Park, J. (2016). Synchronization of Kuramoto oscillators with adaptive couplings. *SIAM Journal on Applied Dynamical Systems*, *15*(1), 162–194. https://doi.org/10.1137/15M101484X

Haider, B., Häusser, M., & Carandini, M. (2013). Inhibition dominates sensory responses in the awake cortex. *Nature*, *493*(7430), 97–100. https://doi.org/10.1038/nature11665

Harris, K. D., & Thiele, A. (2011). Cortical state and attention. *Nature Reviews. Neuroscience*, *12*(9), 509–523. https://doi.org/10.1038/nrn3084

Hartigan, J. A., & Hartigan, P. M. (1985). The dip test of unimodality. *Annals of Statistics*, *13*(1), 70–84. https://doi.org/10.1214/aos/1176346577

Hoefler, T., Alistarh, D., Ben-Nun, T., Dryden, N., & Peste, A. (2021). Sparsity in deep learning: pruning and growth for efficient inference and training in neural networks. *Journal of Machine Learning Research: JMLR*, *22*(1), 10882–11005. https://dl.acm.org/doi/abs/10.5555/3546258.3546499

Holtmaat, A. J. G. D., Trachtenberg, J. T., Wilbrecht, L., Shepherd, G. M., Zhang, X., Knott, G. W., & Svoboda, K. (2005). Transient and persistent dendritic spines in the neocortex in

vivo. *Neuron*, *45*(2), 279–291. https://doi.org/10.1016/j.neuron.2005.01.003

Izhikevich, E. M. (2010). *Dynamical systems in neuroscience: The geometry of excitability and bursting*. The MIT Press. https://doi.org/10.7551/mitpress/2526.001.0001

Kasai, H., Hayama, T., Ishikawa, M., Watanabe, S., Yagishita, S., & Noguchi, J. (2010). Learning rules and persistence of dendritic spines. *The European Journal of Neuroscience*, *32*(2), 241–249. https://doi.org/10.1111/j.1460-9568.2010.07344.x

Klinzing, J. G., Niethard, N., & Born, J. (2019). Mechanisms of systems memory consolidation during sleep. *Nature Neuroscience*, *22*(10), 1598–1610. https://doi.org/10.1038/s41593-019-0467-3

Kuramoto, Y. (1984). *Chemical oscillations, waves, and turbulence*. Springer Berlin Heidelberg. https://doi.org/10.1007/978-3-642-69689-3

Kuramoto, Y. (1975). Self-entrainment of a population of coupled non-linear oscillators. *International Symposium on Mathematical Problems in Theoretical Physics*, 420–422. https://doi.org/10.1007/BFb0013365

Kuroki, S., & Mizuseki, K. (2024). Excitation–inhibition balance controls synchronization in a simple model of coupled phase oscillators. In *Social Science Research Network*. https://doi.org/10.2139/ssrn.4719198

Landmann, N., Kuhn, M., Piosczyk, H., Feige, B., Baglioni, C., Spiegelhalder, K., Frase, L., Riemann, D., Sterr, A., & Nissen, C. (2014). The reorganisation of memory during sleep. *Sleep Medicine Reviews*, *18*(6), 531–541. https://doi.org/10.1016/j.smrv.2014.03.005

Lewis, P. A., Knoblich, G., & Poe, G. (2018). How memory replay in sleep boosts creative problem-solving. *Trends in Cognitive Sciences*, *22*(6), 491–503. https://doi.org/10.1016/j.tics.2018.03.009

Matsuzaki, M., Honkura, N., Ellis-Davies, G. C. R., & Kasai, H. (2004). Structural basis of long-term potentiation in single dendritic spines. *Nature*, *429*(6993), 761–766. https://doi.org/10.1038/nature02617

Miyawaki, H., & Diba, K. (2016). Regulation of hippocampal firing by network oscillations during sleep. *Current Biology*, *26*(7), 893–902. https://doi.org/10.1016/j.cub.2016.02.024

Mizuseki, K., & Buzsáki, G. (2013). Preconfigured, skewed distribution of firing rates in the hippocampus and entorhinal cortex. *Cell Reports*, *4*(5), 1010–1021. https://doi.org/10.1016/j.celrep.2013.07.039

Montbrió, E., & Pazó, D. (2018). Kuramoto model for excitation-inhibition-based oscillations. *Physical Review Letters*, *120*(24), 244101. https://doi.org/10.1103/PhysRevLett.120.244101

Niyogi, R. K., & English, L. Q. (2009). Learning-rate-dependent clustering and self-development in a network of coupled phase oscillators. *Physical Review. E, Statistical, Nonlinear, and Soft Matter Physics*, *80*(6 Pt 2), 066213. https://doi.org/10.1103/PhysRevE.80.066213

Nobre, A. C., & Kastner, S. (Eds.). (2014). *The Oxford Handbook of Attention*. Oxford University Press. https://doi.org/10.1093/oxfordhb/9780199675111.001.0001

Norimoto, H., Makino, K., Gao, M., Shikano, Y., Okamoto, K., Ishikawa, T., Sasaki, T., Hioki, H., Fujisawa, S., & Ikegaya, Y. (2018). Hippocampal ripples down-regulate synapses. *Science*, *359*(6383), 1524–1527. https://doi.org/10.1126/science.aao0702

Park, J., Poyato, D., & Soler, J. (2021). Filippov trajectories and clustering in the Kuramoto model with singular couplings. *Journal of the European Mathematical Society* , *23*(10), 3193–3278. https://doi.org/10.4171/JEMS/1081

Picallo, C. B., & Riecke, H. (2011). Adaptive oscillator networks with conserved overall coupling: Sequential firing and near-synchronized states. *Physical Review. E, Statistical, Nonlinear, and Soft Matter Physics*, *83*(3 Pt 2), 036206. https://doi.org/10.1103/PhysRevE.83.036206

Poyato, D. (2019). Filippov flows and mean-field limits in the kinetic singular Kuramoto model. In *arXiv [math.AP]*. arXiv. http://arxiv.org/abs/1903.01305

Ren, Q., & Zhao, J. (2007). Adaptive coupling and enhanced synchronization in coupled phase

oscillators. *Physical Review. E, Statistical, Nonlinear, and Soft Matter Physics*, *76*(1 Pt 2), 016207. https://doi.org/10.1103/PhysRevE.76.016207

Seliger, P., Young, S. C., & Tsimring, L. S. (2002). Plasticity and learning in a network of coupled phase oscillators. *Physical Review. E, Statistical, Nonlinear, and Soft Matter Physics*, *65*(4 Pt 1), 041906. https://doi.org/10.1103/PhysRevE.65.041906

Tononi, G., & Cirelli, C. (2020). Sleep and synaptic down-selection. *The European Journal of Neuroscience*, *51*(1), 413–421. https://doi.org/10.1111/ejn.14335

Wu, Y. K., Miehl, C., & Gjorgjieva, J. (2022). Regulation of circuit organization and function through inhibitory synaptic plasticity. *Trends in Neurosciences*, *45*(12), 884–898. https://doi.org/10.1016/j.tins.2022.10.006